Atmos. Chem. Phys. Discuss., doi:10.5194/acp-2016-680, 2016
Manuscript under review for journal Atmos. Chem. Phys.
Published: 7 September 2016

Atmospheric Chemistry and Physics
Discussions
Open Access

A new statistical approach to improve the satellite based estimation of the radiative forcing by aerosol- cloud interactions

Piyushkumar N Patel[1], Johannes Quaas[2], Raj Kumar[1]

[1]Space Applications Centre, ISRO, Ahmedabad, India
[2]Institute for Meteorology, Universität Leipzig, Leipzig, Germany

Corresponding to: Piyushkumar N Patel (piyushether@gmail.com)

Abstract

In a previous, study of *Quaas et al., (2008)* the radiative forcing by anthropogenic aerosol due to aerosol-cloud interactions, RF_{aci}, was obtained by a statistical analysis of satellite retrievals using a multilinear regression. Here we employ a new statistical approach to obtain the six fitting parameters, determined using a non-linear statistical approach to obtain the six fitting parameters, for the relationship between planetary albedo and cloud properties and, further, the relationship of the cloud properties and aerosol optical depth. The statistical approach is compared to the results from radiative transfer simulations over three different regions and for different seasons. We find that the results of the new approach agree well with the simulated results over both land and ocean. The new statistical approach increases the correlation coefficient of the fitted to the satellite-retrieved albedo by 21%-23% and decreases the error, compared to the previous approach.

1 Introduction

Aerosols are considered to have a large effect on climate, both through aerosol radiation interactions, and through aerosol-cloud interactions by serving as cloud condensation nuclei (CCN), therefore increasing N_d and thus cloud albedo (*Twomey, 1974*), as well as rapid cloud adjustments (*Boucher et al., 2013*). Much work has been done to quantify the radiative forcing by aerosol-cloud interaction (RF_{aci}), yet it remains highly uncertain. The annual radiative forcing from aerosol induced changes in cloud albedo were reported as -0.7 Wm^{-2} with an uncertainty range -1.8 to -0.3 Wm^{-2} (*Boucher et al., 2013*); this effect could offset much of the warming from greenhouse gases (*Huber and Knutti, 2011*), emphasizing the need to understand the effect so that we can better predict the future climate.

In this study, we concentrate on the RF_{aci}, the change in cloud albedo with increasing aerosol. An increasing aerosol at constant cloud water content is supposed to decrease droplet size, which in turn increases the cloud albedo due to the increase scattering of the smaller, more numerous cloud droplets. *Feingold et al. (2001, 2003); McComiskey et al., (2009)* proposed a metric to quantify the microphysical component of the cloud albedo effect ($ACI = -d\ \ln N_d / d \ln \alpha$), where N_d is the cloud droplet number concentration and α in some proxy for the aerosol burden. Note that the partial derivatives must be calculated at constant liquid water path (LWP). A variety of proxies has been used to represent the cloud response to the change in aerosol, e, g., cloud optical depth (τ_c), cloud drop number concentration (N_d) and r_e. Similarly, various proxies have been used to represent the aerosol particles affecting the cloud, including aerosol number concentration (N_a), aerosol optical depth (τ_a) and aerosol index (AI).

An overview about published relationships and their biases due to mismatches between process- and analysis scales are discussed in *McComiskey and Feingold, (2012)*. Values for ACI metrics from observations often differ significantly from model-based values (*Quaas et al., 2008, 2009; Bellouin et al., 2008; Penner et al., 2011, 2012*). For example, the observational-based values of RF_{aci}, often in the range of -0.2 to -0.6 Wm^{-2} (*Quaas et al., 2008; Bellouin et al.,2013*), is tend to be weaker than the modeled values in the range of -0.5 to -1.9 Wm^{-2} (*IPCC, 2007*). The differences in model and observational-based RF_{aci} have to be reconciled. *Penner et al., (2011)* reported that the lower sensitivities of cloud droplet number concentration, when considering aerosol optical depth (AOD) compared to aerosol index as aerosol quantity may lead to a significant underestimation in satellite-based RF_{aci}. However, *Quaas et al., (2011)* pointed out the weaknesses in the approach used by *Penner et al., (2011)*. Clearly, further study is needed to reduce the uncertainties in both observational- and model-based estimates of aerosol RFaci and to reconcile the differences.

Quaas et al., (2008) derived the anthropogenic aerosol RF_{aci} based on satellite retrievals of aerosol and clouds properties using statistical relationships between cloud properties and anthropogenic aerosols without the use of radiative transfer model. They developed a statistical relationship between planetary albedo and cloud properties using a multilinear fit, and further, the relationships of cloud properties and aerosol optical depth. *Quaas et al. (2008)* suggested that uncertainties in the statistical relationship and fitting parameters introduced uncertainty in the estimate of RF_{aci}. Therefore, it is useful to reassess the estimated RF_{aci} by using a new statistical fitting approach. The main objective of this study is to explore the uncertainty in the satellite-based quantification of RF_{aci}. This study differs from previous studies by introducing new statistical fitting approach to obtain the fitting parameters for the estimates of RF_{aci}, determined using a nonlinear fit between planetary albedo and cloud properties. To verify the present approach, the results from both statistical approaches are compared with the results from a radiative transfer model.

Recent studies suggest that the south Asian region is one of the world's most populous (~24% of the world population) region with growing industrial and transport sectors. A large and increasing power demand, fuel consumption, and equally diverse geographical features make this region among the global hotspots of aerosols. The complex geography of this region contributes significant amounts of natural aerosols (desert dust, pollen, sea-salt etc) into the atmosphere, which mix with anthropogenic ones, making the aerosol environment one of the most complex in the world (*Moorthy et al., 2015*). The large spatial heterogeneity of the sources coupled with the atmospheric dynamics driven by topography and contrasting monsoons, make South Asia's aerosol very difficult to characterize and to model their implications on radiative and climate forcing. While tropospheric perturbations would produce strong regional signatures, their global impacts still remain marginally above the uncertainty levels (*IPCC, 2013*). In the recent years, several studies are carried out on the aerosol characterization and its direct effect over south Asia, but there have been very few studies reported on the aerosol indirect effect using ground- and satellite-based measurements due to complex aerosol and cloud environments. Therefore, we discuss the RF_{aci} for both anthropogenic and natural fraction of aerosol for a period of six-years (2008-2013) for three different regions of south Asia (Arabian Sea (AS; 63°E-72°E, 7°N-19°N), Bay of Bengal (BOB; 85°E-94°E, 7°N-19°N) and Central India (CI; 75°E-84°E, 20°N-30°N)), having significantly distinct aerosol environments as a result of variations in aerosol sources and transport pathways (*Cherian et*

Atmos. Chem. Phys. Discuss., doi:10.5194/acp-2016-680, 2016
Manuscript under review for journal Atmos. Chem. Phys.
Published: 7 September 2016

al., 2013; Das et al., 2015; Tiwari et al., 2015) Additionally, we also discuss the uncertainties of the results in the following sections.

2 Data

We combine measurements of aerosol, cloud and radiative properties to derive the top-of-the atmosphere (TOA) RF_{aci} of both anthropogenic and natural aerosols. Data acquired by sensors mounted on Aqua (*Parkinson, 2003*) and Aura (*Schoeberl et al., 2006*) are used in this study. We use the broadband shortwave planetary albedo (α) (*Wielicki et al., 1996; Loeb, 2004; Loeb et al., 2007*) as retrieved by the Clouds and the Earth's Radiant Energy System (CERES) in combination with cloud properties from the MODerate Resolution Imaging Spectroradiometer (MODIS; *Minnis et al., 2003*) and AOD (τ_a) and fine mode fraction (FMF) as retrieved by the MODIS onboard Aqua (*Remer et al., 2005*). Albedo and cloud properties are from the CERES Single-Scanner-Footprint (SSF) Level-2 Edition-3A data set at 20×20 km^2 horizontal resolution and aerosol properties (AOD and FMF) at 550nm from the MYD04 level-2 collection-5.1 dataset at 10×10 km^2 horizontal resolution are used. We used UV-aerosol index (UV-AI; *Torres et al., 1998*) measured by Ozone Monitoring Instrument (OMI; *Levelt et al., 2006*) onboard Aura from the OMAERUVG level-2 version 003 dataset at 0.25º×0.25º grid, which is a gridded dataset containing retrievals from the OMAERUV (*Torres et al., 2007*) algorithm. The data from CERES and MODIS level-2 products are interpolated to a 0.25º×0.25º regular longitude-latitude grid to separate the aerosol and cloud properties for anthropogenic and natural aerosols using UV-AI. Daily data, taken at roughly 13:30 local time, cover the 2008-2013 period.

3 Methods

All statistics between aerosol and cloud properties are computed separately for 3 regions and for each month of data at 0.25º×0.25º grid resolution. To avoid the greater uncertainty that exists in a clear distinction between aerosols and clouds and accurate retrieval of cloud properties, only single-layer cloud with liquid water path (LWP) > 20 gm^{-2} are taken into account. RF_{aci} for anthropogenic and natural aerosols are calculated using the methods outlined by *Quaas et al., (2008)* with the new statistical approach. As a part of this process, the method by *Kim et al., (2007)* MODIS-OMI algorithm (MOA) is employed to classify the aerosol types into one of four types sea-salt, carbonaceous, dust and sulfate using MODIS FMF and OMI UV-AI data. FMF provides information on the representative size of the aerosol. FMF is close to 1 for mostly small aerosol particles, which implies an anthropogenic origin and FMF becomes small for non-anthropogenic aerosol like dust. UV-AI allows to detect the absorption due to the presence of an aerosol layer by utilizing the sensitivity of absorptive aerosol in UV. Under most condition, UV-AI is positive for absorbing aerosols and negative for non-absorbing aerosols. Using these two independent data sets, aerosol can be classified. Details for the aerosol classification are discussed in *Kim et al., (2007)*. For the purpose of this research, the combination of dust and sea-salt AOD considered as a natural AOD and an anthropogenic AOD contains the combination of carbonaceous and sulfate. Further, the RF_{aci} is estimated for both anthropogenic and natural aerosols.

3.1 Satellite-based estimate of RF_{aci}

RF_{aci} is a function of the relationship between AOD and N_d in a cloud. N_d is not directly provided by satellite product and must be computed using cloud optical thickness (τ_c) and

Atmos. Chem. Phys. Discuss., doi:10.5194/acp-2016-680, 2016
Manuscript under review for journal Atmos. Chem. Phys.
Published: 7 September 2016

Atmospheric Chemistry and Physics
Discussions

effective droplet radius (r_e) for liquid water clouds assuming adiabaticity (*Brenguier et al., 2000*).

$$N_d = \gamma \tau_c^{1/2} r_e^{-5/2} \tag{1}$$

Where, $\gamma = 1.37\times10^{-5}$ $m^{-0.5}$ in this study.
Quaas et al., (2008) is adopted the *Loeb (2004)* approach for the estimate of planetary albedo. Albedo (α) of a cloud scene can be well described by a sigmoidal fit as

$$\alpha \approx (1-f)[a_1 + a_2 ln\tau_a] + f[a_3 + a_4(f\tau_c)^{a_5}]^{a_6} \tag{2}$$

Where, a_1- a_6 are fitting parameters obtained by a multilinear regression, where a_5 is set as 1. Dependency of τ_a is introduced to include the clear part of the scene in the above equation and f is the cloud fraction. The satellite-based estimate of RF_{aci} for anthropogenic and natural aerosols can be expressed as

$$\Delta F_{ant/nat}^{RF_{aci}} = f_{liq}.A(f,\tau_c)\frac{1}{3}\frac{d\ln N_d}{d\ln \tau_a}\left[\ln \tau_a - \ln(\tau_a - \tau_a^{ant/nat})\right] S \tag{3}$$

$$where, A(f,\tau_c) = a_4 a_5 a_6\left[a_3 + a_4(f\tau_c)^{a_5}\right]^{a_6-1}(f\tau_c)^{a_5}$$

RF_{aci} is calculated separately for the anthropogenic and natural aerosols for all three regions for each month. A(f, τ_c) is the empirical function relating albedo to f and τ_c. $\tau_a^{ant/nat}$ is aerosol optical depth for anthropogenic and natural aerosol, respectively, S is the daily mean solar incoming solar radiation.
A goal of the present study is to assess the uncertainty in the satellite-based estimate of the RF_{aci}. For that purpose, we adopted the new statistical nonlinear fitting approach to obtain the six fitting parameters in Eq. (2). Instead of considering a_5=1 in the multiple regression, as in *Quaas et al. (2008),* we obtained the values of all six fitting parameters using a nonlinear fitting approach for each month and region. To get an impression of the performance of our statistical approach, we correlate α and RF_{aci} at TOA obtained from both statistical fitting methods (multilinear and nonlinear) vs. α and RF_{aci} simulated by radiative transfer model for all three regions. The following section describes the detail information about the simulation of α and RF_{aci} using the radiative transfer model.

3.2 Simulation of planetary albedo (α) and RF_{aci}

In order to verify both the statistical approaches, we performed a radiative transfer simulation to obtain α and RF_{aci} for all three regions. Radiative transfer calculations are performed with the SBDART [Santa Barbara DISORT Atmospheric Radiative Transfer; *Ricchiazzi et al., 1998*] that is a plane-parallel radiative transfer code based on the DISORT algorithm for discrete-ordinate-method radiative transfer in multiple scattering and emitting layered media (*Stamnes et al., 1988*). The discrete ordinate method provides a numerically stable algorithm to solve the equations of plane-parallel radiative transfer in a vertically inhomogeneous atmosphere. Simulations are carried out for the solar spectrum (0.2-4.0µm) for all three regions. In the present study, simulations are carried out to simulate first α and later RF_{aci} for the given inputs. Here α is evaluated as the ratio of broadband outgoing (or upwelling) shortwave flux to the incoming (or downwelling) solar flux. Inputs to the model include profiles of temperature and water vapor which are resolved into 32 layers extending from 1000 to 1 mbar and come from European Centre for Medium-range Weather Forecast (ECMWF) reanalysis data. Total columnar amount of atmospheric ozone is provided from OMI-AURA. Surface albedo is set to

Atmos. Chem. Phys. Discuss., doi:10.5194/acp-2016-680, 2016
Manuscript under review for journal Atmos. Chem. Phys.
Published: 7 September 2016

Atmospheric Chemistry and Physics
Discussions

0.15 to represent a typical land cover value for CI and, predefined option of the ocean surface is used for the oceanic regions (AS and BOB). In the SBDART model, the cloud parameter inputs are effective droplet radius (r_e), liquid water path (LWP) and the cloud fraction, all of which are taken from MODIS retrievals reported in the CERES-SSF product. The geometrical thickness of cloud (CGT) is computed as a difference between cloud top and bottom heights. Cloud top height is taken from CERES-SSF product and cloud base height is evaluated using the geopotential height profile from ECMWF data. Only liquid water clouds are considered in the estimation of RF_{aci}. The upwelling and downwelling fluxes are computed individually computed for all three regions at satellite (MODIS-Aqua as a reference) overpass time.
The local radiative forcing associated with the RF_{aci} is estimated as the difference between the perturbed and unperturbed radiative fluxes caused by perturbation in N_d due to the addition of aerosols while keeping the same meteorology. RF_{aci} is diagnosed by making two calls to the radiative transfer code: the first call used the unperturbed satellite-derived N_d and the second used perturbed N_d due to anthropogenic and natural aerosols. The numerical evaluation of radiative flux for the perturbed case starts by determining the finite perturbation of cloud droplet number concentration (ΔN_d), calculated as follows:

$$\Delta N_d^{ant/nat} = \frac{d\ln N_d}{d\ln \tau_a}\,[\ln\tau_a - \ln(\tau_a - \tau_a^{ant/nat})] \tag{4}$$

The finite perturbation in N_d are evaluated separately for anthropogenic and natural aerosol to estimate the radiative flux for the perturbed case. The perturbed value of $\acute{N}_d$ ($N_d + \Delta N_d$) is used to obtain a perturbed value of r_e using Eq. (5) for constant liquid water content because r_e is used as an input to the radiative transfer code.

$$\acute{N}_d = q_l/(\frac{4}{3}\pi {r_e}^3 \rho_w) \tag{5}$$

Where, ρ_w is the liquid water density, q_l the liquid water content (q_l=liquid water path / geometrical thickness). RF_{aci} is diagnosed as $RF_{unperturbed}$ - $RF_{perturbed}$ radiative fluxes at the top of the atmosphere, because increased concentrations of aerosol reduce the effective radius of cloud particles and smaller cloud particles reflect more radiation back to space. The following section describes the details of regression analysis of α and RF_{aci} performed between values from statistical-approaches and simulated values.

4 Results

4.1 Regression analysis

As stated in section 3.1, the satellite-based estimates of RF_{aci} are dependent on the fitting parameters α_1-α_6, obtained here from the two different statistical fitting approaches (multilinear and nonlinear). The parameters obtained from these two approaches are listed in Table-S1 for all three regions investigated in this study. These parameters vary with months since we conducted both the fitting approaches for each month, but only the mean seasonal parameters are shown here. The main differences in fitting parameters from both methods are found in the values of α_4, α_5 and α_6. The weight given to α_4 and α_6 in the nonlinear fit is larger than for the multilinear regression fitting, which may reduce the weight of α_5.
To accomplish the objective of this study, we correlate α and RF_{aci} at TOA obtained from both statistical fitting approaches (multilinear and nonlinear) with estimates obtained from radiative transfer model for all three regions. Fig. 1 shows scatter density plots of comparison between model-simulated albedo and the one computed from satellite measurements at 0.25°×0.25° grid

resolution using both statistical methods for all three regions. This regression analysis suggests that the albedo fitted by the new statistical approach (nonlinear fit) agrees well with the model-simulated albedo over both land and ocean. The scatter of the results from the nonlinear fit around the 1:1 line is much smaller compared to multilinear fit, which is also reflected in the coefficients of determination (R^2) ranging from 0.74 to 0.79. However, a reduction in over and underestimation at very large and very small albedos, respectively, is found in the nonlinear fit compared to the multilinear statistical approach. This is also clearly reflected in the values for the root mean square error (RMSE), which reduces from 0.042-0.065 to 0.010-0.017, supporting the expectation that the new statistical method is more reliable. Additionally, a comparison between the planetary albedo computed using both statistical fits and the CERES retrieved albedo is shown in Fig. S3 for all three regions. Similar to the results discussed above, the analysis shows a good agreement between the CERES derived albedo and the one calculated using the nonlinear fit.

In addition, we performed a comparison of RF_{aci} obtained from satellite measurements using both statistical approaches with the one simulated by SBDART for each season and for each region. Fig. 2 illustrates the linear regression of RF_{aci} from the two statistical approaches plotted against the one obtained from the radiative transfer model for both anthropogenic and natural aerosols for all seasons and all three regions. The analysis showed satisfactory results with Pearson's correlation coefficient r=0.82 and 0.75 and RMSE=0.037 Wm^{-2} and 0.042 Wm^{-2} for anthropogenic and natural fraction of aerosols, respectively. An examination of Fig. 2 reveals that the nonlinear fitting approach reduces the scatter seen for the multilinear fit and the improvement in correlation with the simulated forcing. Using the nonlinear fit increases the correlation coefficient by 21%-23% and decreases the RMSE by from 0.007 $Wm^{-2}$to 0.011 Wm^{-2} compared to multilinear approach.

4.2 RF_{aci} and Uncertainties

Aerosol and clouds vary substantially as a function of time in all regions; thus, it is interesting to analyze aerosol-cloud interactions as a function of season. Fig. 3 shows the seasonal variability of six-year averaged radiative forcing by aerosol-cloud interaction for the three regions as defined above. The maximum anthropogenic RF_{aci} is found over oceanic regions (AS: -0.15Wm^{-2}, BOB: -0.16Wm^{-2}), instead of regions over land (CI: -0.12 Wm^{-2}) with high anthropogenic emissions. This is because maritime clouds are more susceptible to changes in concentration of anthropogenic aerosols (*Quaas et al., 2008*). In contrast, the natural RF_{aci} is generally stronger over land (-0.15 Wm^{-2}) than over oceanic regions (AS: -0.098 Wm^{-2}, BOB: -0.07Wm^{-2}). It is seen that the anthropogenic RF_{aci} is strongest during winter over AS and BOB, with values near -0.19 Wm^{-2} and -0.22Wm^{-2}, whereas it is strong (-0.2 Wm^{-2}) during pre-monsoon over CI (land). The dominance of natural aerosols in pre-monsoon results a large natural RF_{aci} both over land (-0.15 Wm^{-2}) and ocean (-0.098 Wm^{-2} and -0.07 Wm^{-2}).

It is useful to compute the associated uncertainties in the above results due to various parameters. Uncertainty involves the ones due to satellite retrievals of AOD which can be highly biased in the vicinity of cloud due to swelling (*Koren et al., 2007*), and also due to 3D effects (*Wen et al., 2007*). Since both biases may be particularly high for thick clouds, our estimate of the RF_{aci} could be still be overestimated. The uncertainty in MODIS retrievals of AOD from validation studies (*Levy et al., 2007*) was quantified at 0.03+0.05τ_a over ocean and 0.05+0.15τ_a over land. However, since we use the MODIS-OMI algorithm (*Kim et al., 2007*) to estimate the anthropogenic and natural fraction of AOD, uncertainty in this is given as 1σ standard deviations as per Table-S2. From satellite intercomparison, the uncertainty in radiative flux retrievals by CERES is estimated at 5% (*Loeb, 2004*), and uncertainty in cloud optical depth is 21% (*Minnis et al., 2004*). The computed RF_{aci} in this study is closely associated with the statistical fitting approach as described in section 3. As mentioned earlier, two different statistical fitting methods are used to obtain the regression coefficients for the estimates of RF_{aci}. The study showed that the new nonlinear fitting approach reduces by ~20%-25% the uncertainty from the statistical relationship and fitting parameters. The propagation of error yields an influence of these relative uncertainties in the input quantities on the computed RF_{aci} of ~±0.08Wm^{-2}. It should be noted that we refer here to the published quantifiable uncertainties in the satellite retrievals. Limitation involves in this approach or in the satellite measurements contribute to the overall uncertainty but cannot be quantified.

5 Conclusion

In this study, we employed a new nonlinear statistical fitting approach to develop the statistical relationship. A satellite-based algorithm is used to quantify the anthropogenic and natural fraction of aerosol optical depth for the computation of RF_{aci} from satellite retrievals. In order to verify, α and RF_{aci} estimates using the new statistical approach (nonlinear) along with the previous statistical approach (multilinear fit), these are compared with the results obtained from radiative transfer simulations. The results show a better agreement between model-based estimates and the one estimated using the nonlinear approach compared to the multilinear approach. The nonlinear approach relatively increases by 21%-23% the correlation coefficient and decreases by 0.007Wm^{-2} to 0.011 Wm^{-2} the RMSE compared to multilinear approach. The RF_{aci} is found to be consistent with the value found by statistical relationship between aerosol and cloud properties from MODIS and CERES, respectively, and radiative transfer calculations. Further studies using the data retrieved from active remote sensing instruments (lidar and radar) may be useful to test the assumption made in the present study concerning the proxy of aerosol column, the overestimation of AOD over land and deal with the multi-layer clouds.

Acknowledgments

The authors gratefully acknowledge the constant encouragement received from the Director, SAC for carrying out the present research work. Valuable suggestions received from Deputy Director, EPSA, and Head, CVD also gratefully acknowledged. CERES SSF data were obtained from the NASA Langley Research Center Atmospheric Sciences Data Center (ASDC), and MODIS data used in this study were acquired as part of NASA(tm)s Earth Science Enterprise. The MODIS Science Teams developed the algorithms for the AOD retrievals. The data were processed by the MODIS Adaptive Processing System and the Goddard Distributed Active Archive (DAAC). The Dutch-Finnish built OMI instrument is part of the NASA EOS Aura satellite payload. The OMI project is managed by NIVR and KNMI in Netherlands. The OMI data were also obtained from the DAAC. Reanalysis data are from the European Centre for Medium-Range Weather Forecasts. The authors would like to thank the data distribution centers for their support, Markand Oza for helpful discussion, and their family for the continuous motivation. JQ acknowledges funding by the European Research Council (GA no 306284).

Atmos. Chem. Phys. Discuss., doi:10.5194/acp-2016-680, 2016
Manuscript under review for journal Atmos. Chem. Phys.
Published: 7 September 2016

References

Albrecht, B. A. (1989). Aerosols, cloud microphysics, and fractional cloudiness. *Science*, *245*(4923), 1227–1230. doi:10.1126/science.245.4923.1227

Bellouin, N., Jones, A., Haywood, J., & Christopher, S. A. (2008). Updated estimate of aerosol direct Radiative forcing from satellite observations and comparison against the centre climate model. *Journal of Geophysical Research Atmospheres*, *113*(10). doi:10.1029/2007JD009385

Bellouin, N., Quaas, J., Morcrette, J. J., & Boucher, O. (2013). Estimates of aerosol radiative forcing from the MACC re-analysis. *Atmospheric Chemistry and Physics*, *13*(4), 2045–2062. doi:10.5194/acp-13-2045-2013

Brenguier, J.-L., Pawlowska, H., Schüller, L., Preusker, R., Fischer, J., & Fouquart, Y. (2000). Radiative Properties of Boundary Layer Clouds: Droplet Effective Radius versus Number Concentration. *Journal of the Atmospheric Sciences*, *57*(6), 803–821.

Boucher, O., Randall, D., Artaxo, P., Bretherton, C., Feingold, G., Forster, P., et al. (2013) Clouds and aerosols. In: Stocker TF, Qin D, Plattner GK, Tignor M, Allen SK, Boschung J, et al., editors. Climate change 2013: the physical science basis. Contribution of Working Group I to the Fifth Assessment Report of the Intergovernmental Panel on Climate Change. Cambridge, UK, and New York, NY, USA: Cambridge University Press; pp. 571 – 658.

Cherian, R., Venkataraman, C., Quaas, J., Ramachandran, S. (2013). GCM simulations of anthropgenic aerosol-induced cahnges in aerosol extinction, atmiospheric heating and precepitaion over India. *Journal of Geophysical Research Atmospheres*, 11:2938–2955. doi:10.1002/jgrd.50298

Das, S., Dey, S., and Dash, S. K. (2015). Direct radiative effects of anthropogenic aerosols on Indian summer monsoon circulation. *Theoretical and Applied Climatology*, doi: 10.1007/s00704-015-1444-8

Feingold, G., Remer, L. A., Ramaprasad, J., and Kaufman, Y. J. (2001). Analysis of smoke impact on clouds in Brazilian biomass burning regions: An extension of Twomey's approach. *Journal of Geophysical Research*, *106*, 22907–22922.

Feingold, G., Eberhard, W. L., Veron, D. E., and Previdi, M. (2003). First measurements of the Twomey indirect e ff ect using ground-based remote sensors, *Geophysical Research Letters*, *30*, 1287, doi:10.1029/2002GL016633.

Huber, M., & Knutti, R. (2011). Anthropogenic and natural warming inferred from changes in Earth's energy balance. *Nature Geoscience*. doi:10.1038/ngeo1327

Intergovernmental Panel on Climate Change (IPCC) (2007), Climate Change 2007: The Physical Scientific Basis, edited by S. Solomon et al., Cambridge Univ. Press, New York.

Kim, J., Lee, J., Lee, H. C., Higurashi, A., Takemura, T., & Song, C. H. (2007). Consistency of the aerosol type classification from satellite remote sensing during the Atmospheric Brown Cloud-East Asia Regional Experiment campaign. *Journal of Geophysical Research Atmospheres*, *112*(22). doi:10.1029/2006JD008201

Koren, I., Remer, L. A., Kaufman, Y. J., Rudich, Y., & Martins, J. V. (2007). On the twilight zone between clouds and aerosols. *Geophysical Research Letters*, *34*(8). doi:10.1029/2007GL029253

Levelt, P. F., Van Den Oord, G. H. J., Dobber, M. R., Mälkki, A., Visser, H., De Vries, J., … Saari, H. (2006). The ozone monitoring instrument. *IEEE Transactions on Geoscience and Remote Sensing*, *44*(5), 1093–1100. doi:10.1109/TGRS.2006.872333

Levy, R. C., Remer, L. A., Mattoo, S., Vermote, E. F., & Kaufman, Y. J. (2007). Second-generation operational algorithm: Retrieval of aerosol properties over land from inversion of Moderate Resolution Imaging Spectroradiometer spectral reflectance. *Journal of Geophysical Research Atmospheres*, *112*(13). doi:10.1029/2006JD007811

Atmos. Chem. Phys. Discuss., doi:10.5194/acp-2016-680, 2016
Manuscript under review for journal Atmos. Chem. Phys.
Published: 7 September 2016

Atmospheric Chemistry and Physics Discussions

Loeb, N.: Angular models: Instantaneous and ensemble accuracy, in: 1st CERES-II Science Team Meeting Proceedings, NCAR, Boulder, Colorado, USA, 2004.

Loeb, N. G., B. A. Wielicki, W. Su, K. Loukachine, W. Sun, T. Wong, K. J. Priestley, G. Matthews, W. F. Miller, and R. Davies (2007), Multi-instrument comparison of top-of-atmosphere reflected solar radiation, J. Clim., 20, 575–591.

McComiskey, A., Feingold, G., Frisch, A. S., Turner, D. D., Miller, M. A., Chiu, J. C., Min, Q., and Ogren, J. A. (2009). An assessment of aerosol-cloud interactions in marine stratus clouds based on surface remote sensing. *Journal of Geophysical Research*, *114*, D09203, doi:10.1029/2008JD011006.

McComiskey, A., Feingold, G. (2012). The scale problem in quantifying aerosol indirect effects. *Atmospheric Chemistry and Physics*, *12(2)*, 1031–1049.

Minnis, P., D. F. Young, S. Sun-Mack, P. W. Heck, D. R. Doelling, and Q. Z. Trepte (2003), CERES cloud property retrievals from imagers on TRMM, Terra, and Aqua, in Proc. SPIE 10th International Symposium on Remote Sensing: Conference on Remote Sensing of Clouds and the Atmosphere VII, vol. 5235, pp. 37–48, Barcelona, Spain.

Minnis, P., D. F. Young, S. Sun-Mack, Q. Trepte, D. R. Doelling, D. A. Spangenberg, and P. W. Heck (2004), Ceres cloud products, in 1st CERES-II Science Team Meeting Proceedings, NCAR, Boulder, Colorado.

Moorthy, K.K., et al. (2015). South Asian aerosols in perspective: Preface to the special issue. Atmospheric Environment, http://dx.doi.org/10.1016/j.atmosenv.2015.10.073.

Parkinson, C. L. (2003). Aqua: An earth-observing satellite mission to examine water and other climate variables. *IEEE Transactions on Geoscience and Remote Sensing*, *41*, 173–183. doi:10.1109/TGRS.2002.808319

Penner, J. E., Xu, L., & Wang, M. (2011). Satellite methods underestimate indirect climate forcing by aerosols. *Proceedings of the National Academy of Sciences of the United States of America*, *108*(33), 13404–13408. doi:10.1073/pnas.1018526108

Penner, J. E., Zhou, C., & Xu, L. (2012). Consistent estimates from satellites and models for the first aerosol indirect forcing. *Geophysical Research Letters*, *39*(13). doi:10.1029/2012GL051870

Quaas, J., Boucher, O., Bellouin, N., & Kinne, S. (2008). Satellite-based estimate of the direct and indirect aerosol climate forcing. *Journal of Geophysical Research: Atmospheres*, *113*(5), 1–9. doi:10.1029/2007JD008962

Quaas, J., Boucher, O., & Bréon, F. M. (2004). Aerosol indirect effects in POLDER satellite data and the Laboratoire de Météorologie Dynamique-Zoom (LMDZ) general circulation model. *Journal of Geophysical Research D: Atmospheres*, *109*(8). doi:10.1029/2003JD004317

Quaas, J., Ming, Y., Menon, S., Takemura, T., Wang, M., Penner, J. E., … Schulz, M. (2009). Aerosol indirect effects – general circulation model intercomparison and evaluation with satellite data. *Atmospheric Chemistry and Physics*, *9*(22), 8697–8717. doi:10.5194/acp-9-8697-2009

Quaas, J., O. Boucher, N. Bellouin, and S. Kinne (2011), Which of satellite- or model-based estimates is closer to reality for aerosol indirect forcing?, Proc. Natl. Acad. Sci. U.S.A., 108, E1099.

Remer, L. A., Kaufman, Y. J., Tanré, D., Mattoo, S., Chu, D. A., Martins, J. V., … Holben, B. N. (2005). The MODIS Aerosol Algorithm, Products, and Validation. *Journal of the Atmospheric Sciences*, *62*(4), 947–973. doi:10.1175/JAS3385.1

Ricchiazzi, P., Yang, S., Gautier, C., & Sowle, D. (1998). SBDART: A Research and Teaching Software Tool for Plane-Parallel Radiative Transfer in the Earth's Atmosphere. *Bulletin of the American Meteorological Society*, *79*(10), 2101–2114.

Schoeberl, M. R., Douglass, A. R., Hilsenrath, E., Bhartia, P. K., Beer, R., Waters, J. W., …

Atmos. Chem. Phys. Discuss., doi:10.5194/acp-2016-680, 2016
Manuscript under review for journal Atmos. Chem. Phys.
Published: 7 September 2016

DeCola, P. (2006). Overview of the EOS aura mission. *IEEE Transactions on Geoscience and Remote Sensing*, *44*(5), 1066–1072. doi: 10.1109/TGRS.2005.861950

Stamnes, K., Tsay, S. C., Wiscombe, W., & Jayaweera, K. (1988). Numerically stable algorithm for discrete-ordinate-method radiative transfer in multiple scattering and emitting layered media. *Applied Optics*, *27*(12), 2502–2509. doi:10.1364/AO.27.002502

Tiwari, S., Mishra, A. K., and Singh, A K. (2015). Aerosol climatology over the Bay of Bengal and Arabian Sea inferred from sapce-borne radiometers and lidar observations. *Aerosol and Air Quality Research*, doi:10.4209/aaqr.2015.06.0406.

Torres, O., Bhartia, P. K., Herman, J. R., Ahmad, Z., & Gleason, J. (1998). Derivation of aerosol properties from satellite measurements of backscattered ultraviolet radiation: Theoretical basis. *Journal of Geophysical Research: Atmospheres*, *103*(D14), 17099–17110. doi: 10.1029/98JD00900

Twomey, S. (1977). The Influence of Pollution on the Shortwave Albedo of Clouds. *Journal of the Atmospheric Sciences*.

Wen, G., Marshak, A., Cahalan, R. F., Remer, L. A., & Kleidman, R. G. (2007). 3-D aerosol-cloud radiative interaction observed in collocated MODIS and ASTER images of cumulus cloud fields. *Journal of Geophysical Research Atmospheres*, *112*(13). doi:10.1029/2006JD008267

Wielicki, B. A., Barkstrom, B. R., Harrison, E. F., Lee, R. B., Smith, G. L., & Cooper, J. E. (1996). Clouds and the Earth's Radiant Energy System (CERES): An Earth Observing System Experiment. *Bulletin of the American Meteorological Society*, *77*(5), 853–868.

Atmos. Chem. Phys. Discuss., doi:10.5194/acp-2016-680, 2016
Manuscript under review for journal Atmos. Chem. Phys.
Published: 7 September 2016

Atmospheric Chemistry and Physics
Discussions
Open Access

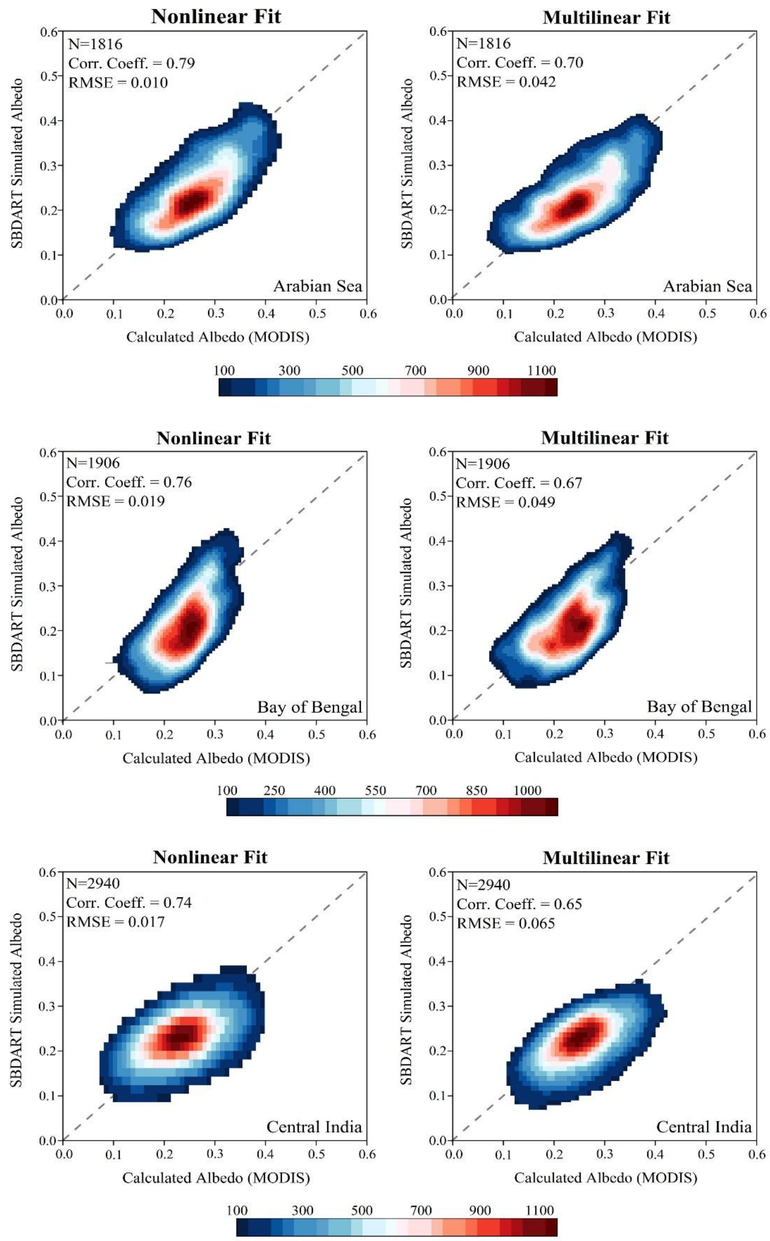

Figure 1. Scatter density plots of model-simulated albedo and the one computed using both statistical fitting method (nonlinear and multilinear fit) using satellite measurements for all three regions.

Atmos. Chem. Phys. Discuss., doi:10.5194/acp-2016-680, 2016
Manuscript under review for journal Atmos. Chem. Phys.
Published: 7 September 2016

Atmospheric Chemistry and Physics
Discussions

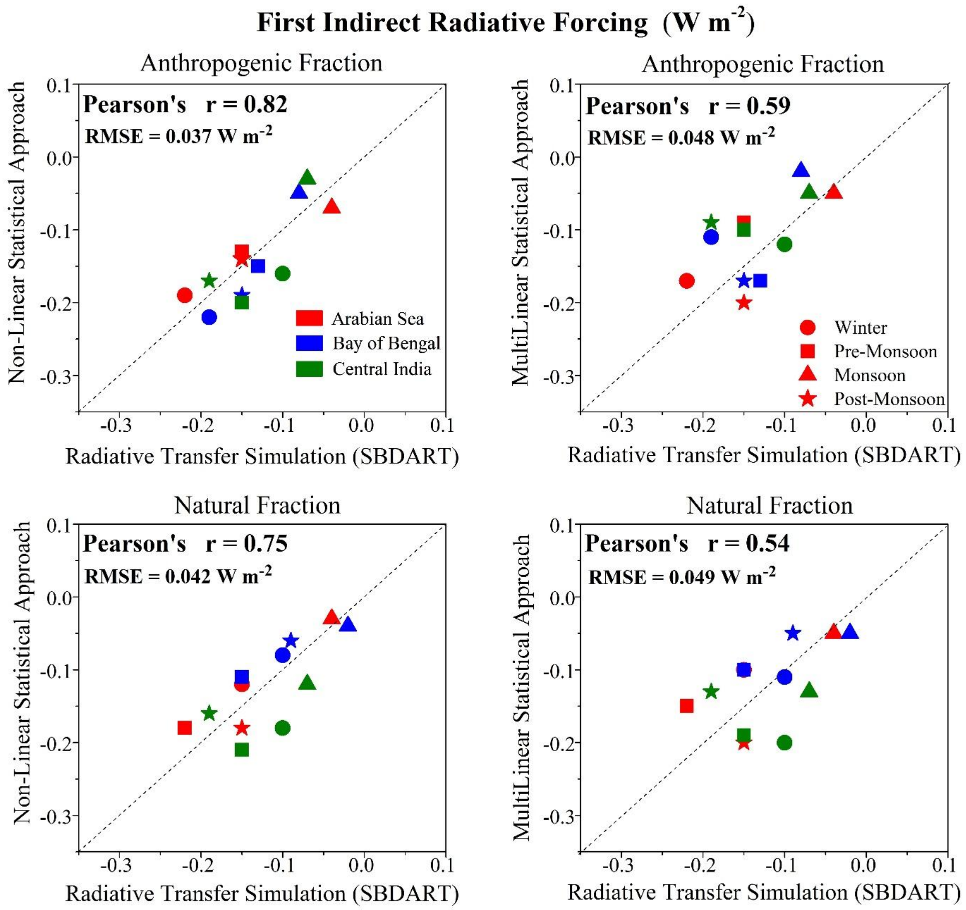

Figure 2. Comparison between satellite-based RF_{aci} using both statistical fits and the one simulated by the SBDART model for all three regions and for all seasons. The different color indicates the regions, whereas the different symbols indicates the different seasons. Note that the fit is separately performed for each season and each region.

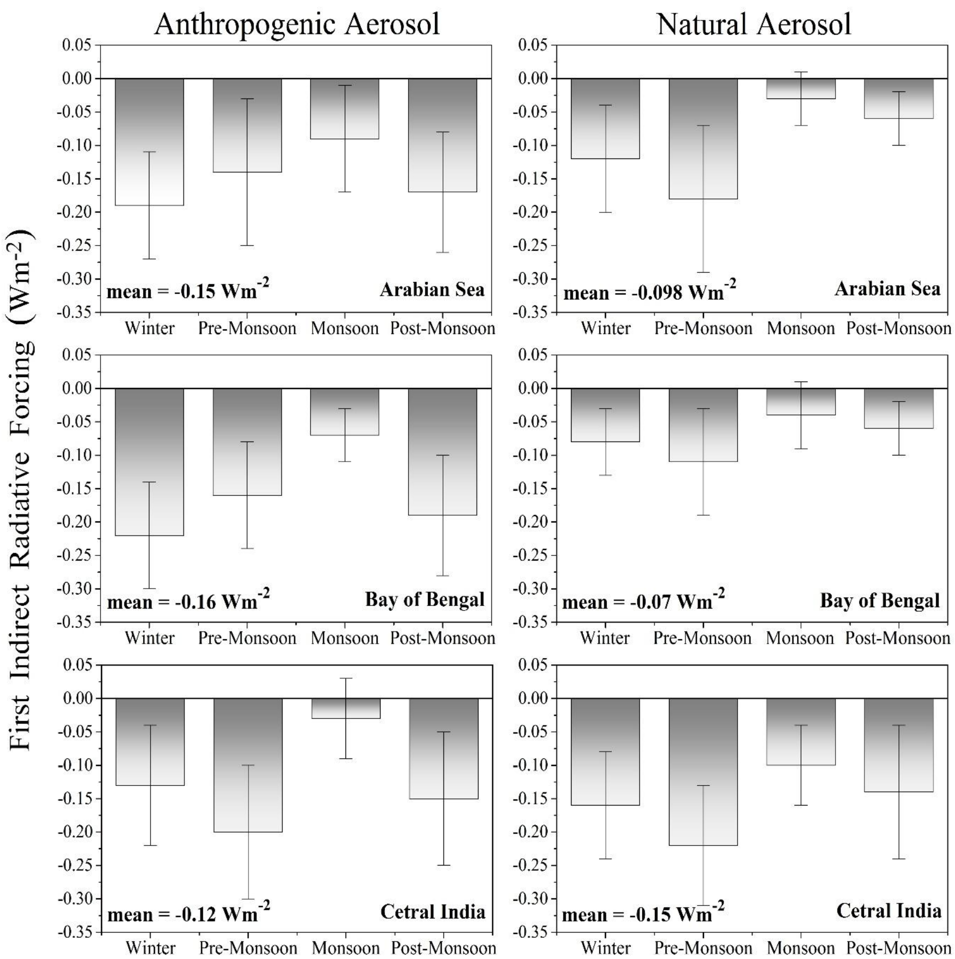

Figure 3. Seasonal variability of six-year averaged RF_{aci} obtained using the nonlinear fit for all three regions for both anthropogenic and natural aerosols along with mean values.